Unraveling the Preparatory Processes of the 2023 M_w 7.8–7.6 Kahramanmaraş Earthquake Doublet

Fengling Yin[1] and Changsheng Jiang*[1]

Abstract

Within a span of 9 hr on 6 February 2023, two significant earthquakes, with magnitudes of M_w 7.8 and 7.6, struck the southeastern part of Türkiye and the northern region of Syria, resulting in significant casualties and widespread economic losses. The occurrence of such intense earthquakes in rapid succession on adjacent faults, especially within a highly complex intraplate region with a multifault network, poses a rare phenomenon, presenting new challenges for seismic hazard analysis in such areas. To investigate whether the preparatory processes for the M_w 7.8–7.6 earthquake doublet could be identified on a large spatial scale prior to the seismic events, we employed a data-driven approach for *b*-value calculation. The difference in *b*-values from the background values (Δb) in a reference period were used as inputs, and the cumulative migration pattern (CMP) method, quantitatively describing the migration of seismic activity, was utilized to calculate the corresponding probability distributions. The results indicate a widespread phenomenon of decreasing *b*-values in the study area over a decade before the occurrence of the earthquake doublet, revealing a significant enhancement of differential crustal stress over a large region. In addition, despite not being the region with the most pronounced decrease in *b*-values, there is a distinct high probability distribution of CMP near the nucleation points of the earthquake doublet, indicating a spatial and temporal "focus" of increased crustal differential stress in the study area, unveiling the preparatory process of the earthquake doublet. This study reveals quantifiable migration patterns over a long time scale and a large spatial extent, providing new insights into the evolution and occurrence processes of the 2023 M_w 7.8–7.6 Kahramanmaraş earthquake doublet. Moreover, it offers potential clues for seismic hazard analysis in such intraplate regions with multiple fault systems.

Cite this article as Yin, F., and C. Jiang (2024). Unraveling the Preparatory Processes of the 2023 M_w 7.8–7.6 Kahramanmaraş Earthquake Doublet, *Seismol. Res. Lett.* **95**, 730–741, doi: 10.1785/0220230413.

Supplemental Material

Introduction

On 6 February 2023, a doublet of strong earthquakes with magnitudes of M_w 7.8 and 7.6 occurred within a span of 9 hr in the Nurdağı-Pazarcık region near the northwestern part of the Kahramanmaraş-Gaziantep Province in southern Türkiye, as well as in neighboring northwestern Syria (Fig. 1a). These earthquakes destroyed or severely damaged approximately 160,000 buildings, resulting in over 50,000 deaths and displacing 200,000 people in Türkiye and Syria, and the affected population reached 14 million (Barbot *et al.*, 2023). The influence of various factors, especially significant long-period seismic motion (Wu *et al.*, 2023) and the complexity of earthquake rupture (Goldberg *et al.*, 2023; Okuwaki *et al.*, 2023; Xu *et al.*, 2023; Zhang *et al.*, 2023), played a crucial role in the severe disaster losses caused by the 2023 M_w 7.8–7.6 Kahramanmaraş earthquake doublet. The rupture of the first earthquake (M_w 7.8) was initiated on the Nurdağı-Pazarcık fault, a southern branch of the east Anatolian fault (EAF), subsequently triggering the rupture of the EAF (Reitman *et al.*, 2023). The rupture propagated initially northeastward along the EAF and then southwestward, spanning the entire southern segment of the fault (Gabriel *et al.*, 2023; Jia *et al.*, 2023; Melgar *et al.*, 2023; Toker *et al.*, 2023; Wang *et al.*, 2023). The second earthquake (M_w 7.6) occurred on the Savrun-Çardak fault, which extends in an east-west direction and has a rupture length of approximately 150 km (Barbot *et al.*, 2023). Although cases of consecutive major earthquakes occurring on adjacent faults have been observed in the past, the occurrence of this earthquake doublet with only a 9 hr separation is exceptionally rare (Mai *et al.*, 2023). Current research

1. Institute of Geophysics, China Earthquake Administration, Beijing, China, https://orcid.org/0000-0002-6812-1875 (CJ)

*Corresponding author: jiangcs@cea-igp.ac.cn

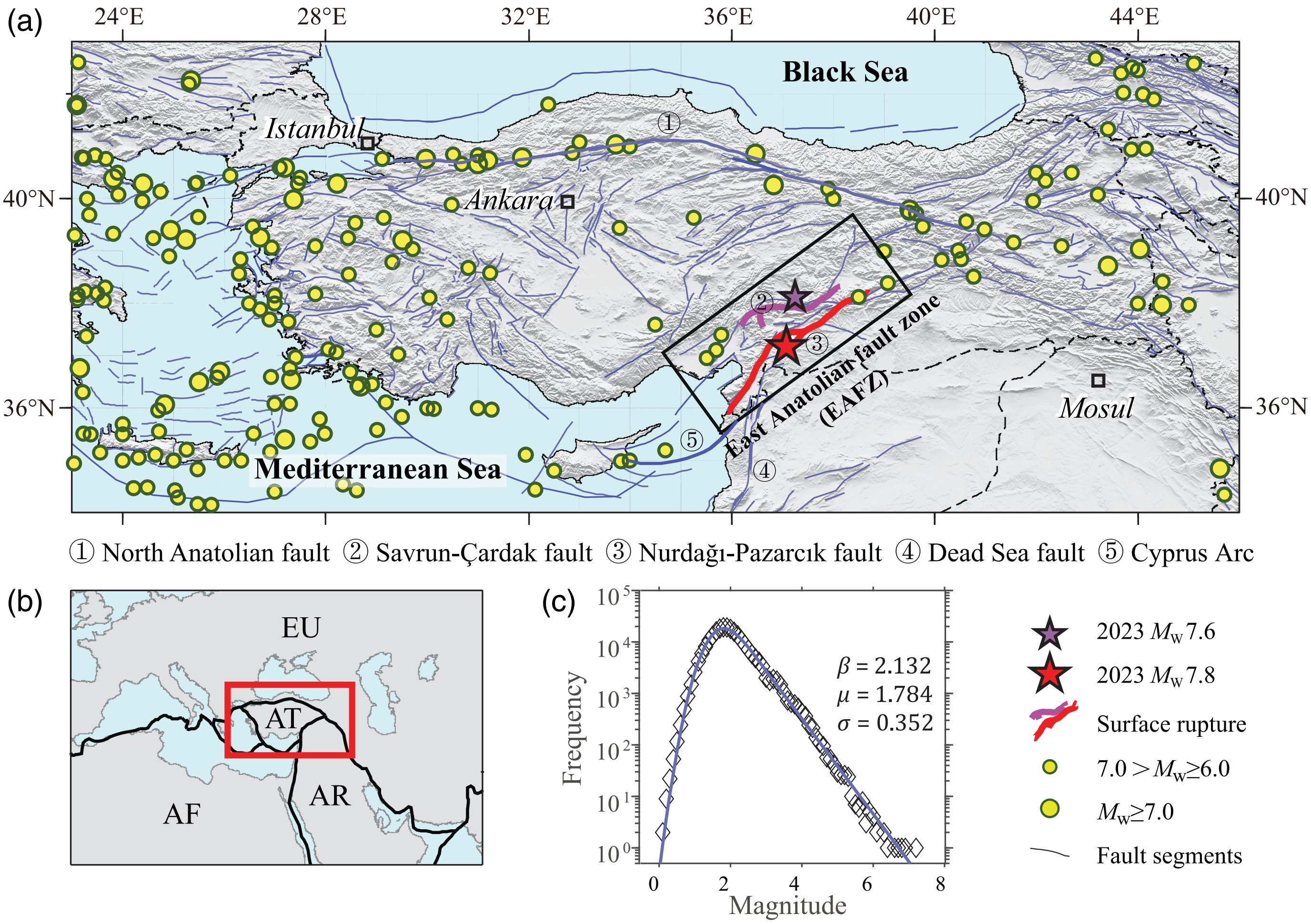

Figure 1. Tectonic setting and seismic activity of the study area. (a) Distribution of earthquakes with magnitude $M_w \geq 6.0$ leading up to the occurrence of the 2023 earthquake doublet. The positions of the 2023 M_w 7.8–7.6 Kahramanmaraş earthquake doublet are indicated by two stars. The bold red and purple lines represent the surface ruptures of the M_w 7.8–7.6 earthquake doublet. The yellow circles denote the M_w 6.0 earthquakes (see Data and Resources). The fault data come from Styron and Pagani (2020). The major faults in Anatolia and main segments of the east Anatolian fault zone plotted on this map refer to Duman and Emre (2013) and Şaroğlu *et al.* (1992); (b) A spatial illustration of the study area's location and tectonic plate boundaries. The study area is outlined in red. Key plate abbreviations: AT, Anatolia plate; AF, Africa plate; AR, Arabia plate; EU, Eurasia plate. (c) Seismic magnitude–frequency distribution for the study area from 6 February 2013 until the occurrence of the earthquake doublet, along with the fitting results obtained using the OK1993 model (Ogata and Katsura, 1993). The black diamonds are the real distribution. The blue curve indicates the fitting results using the OK1993 model. The fitted parameters, [β, μ, σ], are marked on the panel.

suggests that the second event was influenced by the static Coulomb stress changes and dynamic triggering induced by the first event (Ding, Xu, *et al.*, 2023; Jia *et al.*, 2023; Liu *et al.*, 2023; Rebetsky, 2023; Stein *et al.*, 2023).

The 2023 M_w 7.8–7.6 Kahramanmaraş earthquake doublet occurred on the east Anatolian fault zone (EAFZ), situated at the intersection of the Anatolian plate, Arabian plate, and African plate (Fig. 1b). In this region, there are localized and pronounced variations in crustal thickness, displaying a clear correlation with fault zones (Fichtner *et al.*, 2013; Vanacore *et al.*, 2013; Confal *et al.*, 2020; Wang *et al.*, 2020; Eken *et al.*, 2021). The EAF, stretching approximately 600 km, is a large left-lateral strike-slip fault, intersecting with the north Anatolian fault (NAF) to the north and extending southward to the Dead Sea fault and Cyprus Arc (Duman and Emre, 2013; Simonov and Zakharov, 2023), with a slip rate of 10 mm/yr (Aktug *et al.*, 2016). As a complex intracontinental boundary fault, the EAF, along with the NAF, defines the southeastern and north boundaries of the Anatolian plate, which is being pushed westward from the Arabian-Eurasian collision zone (Lyberis *et al.*, 1992; Şaroğlu *et al.*, 1992; Duman and Emre, 2013; Köküm and İnceöz, 2018; Pousse-Beltran *et al.*, 2020). The EAFZ region has witnessed frequent moderate earthquakes of $M_w \geq 4.0$ since the advent of modern instrumental records, and distributed deformations are observed on multiple fault segments (Taymaz *et al.*, 1991; Bulut *et al.*, 2012; Bayrak *et al.*, 2015;

Hussain *et al.*, 2018; Taymaz *et al.*, 2021; Karabulut *et al.*, 2023). Despite several significant earthquakes along the EAFZ since 1900, including the 1905 M_w 6.8, 1971 M_w 6.7, 2010 M_w 6.1, and 2020 M_w 6.7 events, none have exceeded a magnitude of M_w 7.0, and all have been confined to the northwest segment of the EAFZ (Taymaz *et al.*, 2021; Güvercin *et al.*, 2022). Although $M_w \geq 7.0$ events, including the 1893 M_w 7.1 earthquake, occurred in the southern segment of the EAFZ before the twentieth century, the rupture scale of these earthquakes was limited by the geometric curvature of the respective fault (Taymaz *et al.*, 1991; Duman and Emre, 2013), and the phenomenon of consecutive ruptures across multiple fault segments with adjacent faults rupturing within hours, as observed in the current earthquake doublet, was not present. The occurrence of the 2023 M_w 7.8–7.6 Kahramanmaraş earthquake doublet poses significant challenges to seismic hazard analysis in the EAFZ region.

The anticipation and understanding of the preparatory processes leading up to large earthquakes on a regional scale are crucial for policymakers to implement measures to mitigate casualties and economic damage (Hall, 2023). However, current understanding of earthquake preparation processes is often based on a simplified concept of constant rate loading along subduction zone plate boundaries leading to earthquake occurrences and the semiperiodic release of accumulated strain energy. Such a framework is inadequate for unraveling the complex seismic preparation processes in regions like the EAFZ or within continental interiors, in which challenges arise in explaining the long-distance migration of large earthquakes between mechanically coupled fault systems (Liu *et al.*, 2011). Moreover, identifying migration pattern phenomena related to earthquake preparation presents a substantial challenge for urgently assessing the timing and likelihood of future strong earthquakes. Some recent endeavors have attempted to address these challenges in specific seismic cases. For instance, Panet *et al.* (2018) utilized GRACE satellite data to identify dynamic variations in Earth's gravity field and mass several months prior to the 2011 M_w 9.0 Tohoku earthquake in northeastern Japan, suggesting that aseismic expansion at mid-upper mantle depths contributed to the acceleration of subduction and potentially offered insights into future earthquake locations and hazards. Wu *et al.* (2008) pioneered a technique for quantifying the migration patterns based on the seismicity anomaly hot spots and the temporal evolution of "error distances" to the future epicenter. This technique has been applied to seismic cases such as the 2006 M_L 6.4 and 6.7 earthquake doublet in Pingdong, Taiwan region (Wu *et al.*, 2008), and the 2011 M_w 9.0 Tohoku earthquake (Kawamura *et al.*, 2013).

Several clues have emerged about the preparatory processes preceding the 2023 M_w 7.8–7.6 Kahramanmaraş earthquake doublet. For instance, Nalbant *et al.* (2002) calculated stress evolution on the EAFZ since 1822 due to tectonic loading, identifying a high-risk fault segment south of Karamanmaraş that could potentially experience a strong earthquake with a magnitude up to M_w 7.3. Zaccagnino *et al.* (2023) discovered globally clustered, locally Poissonian seismicity and low b-values in the EAFZ region prior to the earthquake doublet. Picozzi and Iaccarino (2023) employed seismic activity analysis to reveal the gradual migration of earthquake frequency and average energy toward the future epicenter within a 300 km radius for the 300 days leading up to the earthquake doublet. However, these studies were limited in their ability to comprehensively describe the seismic preparatory processes on a large spatial scale. In addition, Ding, Zhou, *et al.* (2023) revealed through a study on the detection and identification of preseismic microseismicity that no direct foreshocks were observed in the nucleation zones of the M_w 7.8 and 7.6 earthquakes. This poses new challenges to understanding the preparatory processes of this seismic doublet. In this article, we address the seismic preparatory processes of the 2023 M_w 7.8–7.6 Kahramanmaraş earthquake doublet through two technical advancements and a systematic study of migration patterns. First, we explore the spatial heterogeneity and temporal evolution of differential stress distribution in the EAFZ using b-values derived from the magnitude–frequency relationship. To enhance the reliability of b-value calculations and reduce subjectivity in data selection, we introduce an improved computation technique based on data-driven ideas and model selection using the Bayesian information criterion (BIC). Second, we employ the spatial distribution of b-values as input data for calculating the migration patterns. Drawing inspiration from Wu *et al.* (2008), we quantify the degree of migration patterns and spatial distribution through a cumulative migration pattern (CMP) method developed by Jiang and Wu (2011). These enhancements yield a comprehensive spatiotemporal description of the seismic preparatory processes leading up to the 2023 M_w 7.8–7.6 Kahramanmaraş earthquake doublet.

Materials and Methods

Data-driven approach for *b*-value calculation

Traditional methods for calculating the b-value often rely on subjective data selection, either by setting fixed radii or a predetermined number of seismic events (Smith, 1981; Gulia and Wiemer, 2019), leading to issues of subjectivity and unreliable outcomes. To address subjectivity in data selection, we adopt a data-driven approach for b-value calculation (Si and Jiang, 2019; Jiang *et al.*, 2021). In this approach, we model the magnitude–frequency distribution (MFD) using the continuous function form of the OK1993 model (Ogata and Katsura, 1993),

$$\lambda(m) = \lambda_0(m)q(m), \tag{1}$$

$$\lambda_0(m|\beta) = \exp(-\beta m), \tag{2}$$

in which m represents magnitude, and $q(m)$ is the detection rate function, ranging from 0 to 1, which describes the probability of detecting earthquake events of different magnitudes. The $q(m)$ is formulated as a cumulative normal distribution

$$q(m|\mu,\sigma) = \frac{1}{\sqrt{2\pi\sigma^2}}\int_{-\infty}^{m} e^{-\frac{(x-\mu)^2}{2\sigma^2}}dx, \quad (3)$$

in which m indicates the maximum magnitude of the earthquake catalog for calculation. μ represents the magnitude corresponding to a 50% detection rate, and σ indicates the corresponding magnitude range, typically used to describe the spatiotemporal variability of earthquake detection by seismic networks. Hence, the observed earthquake probability density function is given by

$$\begin{aligned} P(m|\beta,\mu,\sigma) &= \frac{e^{-\beta m}q(m|\mu,\sigma)}{\int_{-\infty}^{+\infty} e^{-\beta m}q(m|\mu,\sigma)dm} \\ &= e^{-\beta m}q(m|\mu,\sigma)/e^{(-\beta\mu+\beta^2\sigma^2/2)}/\beta \\ &= \beta e^{-\beta(m-\mu)-\beta^2\sigma^2/2}q(m|\mu,\sigma). \end{aligned} \quad (4)$$

For a series of observed earthquake magnitudes, the log-likelihood function of the OK1993 model is

$$\ln L(\theta) = n\ln\beta - \sum_{i=1}^{n}[\beta m_i - \ln q(m_i|\mu,\sigma)] + n\beta\mu - \frac{n}{2}\beta^2\sigma^2. \quad (5)$$

By employing maximum-likelihood estimation, we can fit the parameters [β, μ, σ] of the OK1993 model and subsequently calculate the b-value based on the power law relationship.

The key steps in the data-driven b-value calculation method involve the construction of a spatial random model and model selection. First, we specify the number of spatial grid partitions N_v, and the number of random realizations n. We employ Voronoi Tessellation to randomly partition the study area, creating a large number ($N_v \times n$) of spatial random models. Second, we fit the OK1993 model parameters [β, μ, σ] for seismic events within each Voronoi polygon and compute the BIC for each spatial random model. Finally, we select a certain proportion of spatial random models with the smallest BIC values and calculate the ensemble median of b-values as the final result.

CMP method

To quantitatively describe the migration pattern phenomenon of seismic activity at a large spatial scale, we employed the error distance integration method as proposed by Wu *et al.* (2008). This approach defines the error distance ε of seismicity anomalies, referred to as "hot spots," as exceeding a threshold relative to any given spatial target location x_i. It also calculates the area AH occupied by hot spots exceeding a dynamically changing threshold and the spatial coverage ratio $f = AH/A$, in which A represents the total area of the study region. In contrast to the pattern informatics anomalies used by Wu *et al.* (2008) and the accelerating moment release anomalies employed by Jiang and Wu (2011) as hot spots, this study defines hot spots as the difference Δb between the b-values of each time interval and the background seismicity period.

To mitigate the influence of distant hot spots, a Gaussian kernel function is applied to smooth the distances r from the hot spots to the target location x_i,

$$k(r,r_0,c) = e^{-\frac{(r-c)^2}{2r_0}}, \quad (6)$$

in which r_0 represents the reference distance for smoothing and the constant c is set to 0, implying no smoothing for hot spots at the reference point. The error distance ε_j for the jth hot spot with respect to location x_i is defined as $\varepsilon_j = 1 - k_j$. Thus, the average error distance under a specific threshold coverage f can be expressed as

$$\varepsilon_f = \frac{1}{n_f}\sum_{j=1}^{n_f}\left(1 - e^{-\frac{r_j^2}{2r_0^2}}\right), \quad (7)$$

in which r_j is the distance from the jth hot spot to x_i, and n_f is the number of hot spots corresponding to the coverage f. After smoothing and normalization through the Gaussian function, ε becomes a dimensionless variable.

The integration of the ε–f curve yields the integrated error distance $\varepsilon_{\text{area}}(T)$ for a specific time scale T. Subsequently, by progressively reducing T and approaching the mainshock's occurrence time, linear regression is applied to $\varepsilon_{\text{area}}(T)$. The presence of a migration pattern is determined based on the slope. Furthermore, we adopted the quantitative CMP method as outlined by Jiang and Wu (2011) to assess the extent of the migration pattern. We assume that any spatial reference point x_i is a potential nucleation point for rupture, and we calculate $\varepsilon_{\text{area}}(T)$ at that location. The slopes of $\varepsilon_{\text{area}}(T)$ are spatially normalized and represented in probabilistic form (*Prob*), indicating the degree of cumulative seismic migration.

Data collection and processing

In this study, we employed an earthquake catalog from the Kandilli Observatory and Earthquake Research Institute (KOERI) as our primary data source. KOERI operates one of Türkiye's two national seismic networks, which has gradually expanded since the early 1970s. At present, the network encompasses 135 broadband seismic stations, 93 strong-motion stations, and 14 short-period seismic stations. The KOERI earthquake catalog has historically employed the duration magnitude (M_d) as a metric for earthquake size, a practice that continued until 2012, when the local magnitude (M_L) scale was adopted. For larger earthquake events, the M_w magnitudes are concurrently recorded (Kalafat *et al.*, 2011). However, the change in magnitude scales within the KOERI earthquake catalog, specifically the shift from M_d to M_L after 2012, introduces the potential for inconsistencies in earthquake catalog data, thereby affecting the calculation of seismic activity parameters.

For instance, research by Cambaz *et al.* (2019) demonstrated that the minimum complete magnitude M_c 2.7 in the M_d catalog using the earthquakes between the time interval 1 January 2008 to ∼31 December 2011 had a corresponding b-value of 1.65 ± 0.01, and M_c 2.0 in the M_L catalog for the time period 1 January 2012 to ∼31 December 2018 had a b-value of 0.83 ± 0.01. Although the impact of this abrupt magnitude scale transition can be mitigated to some extent by establishing empirical relationships between M_d and M_L, it nevertheless introduces a significant level of uncertainty. To circumvent the influence of earthquake catalog inconsistencies on our calculation results, we exclusively utilized data spanning from 6 February 2013, up until the occurrence of the M_w 7.8–7.6 earthquake doublet. This restricted time frame aims to ensure that our analysis is conducted within a period less impacted by the magnitude scale shift, thereby maintaining the reliability of our findings.

In this section, we delineate the scope of our study within the geographical coordinates of 23° to ∼46° E and 34° to ∼43° N. From the KOERI earthquake catalog, we retrieved a total of 227,216 seismic events that occurred during the study period, and their MFD is depicted in Figure 1c. We employed the OK1993 model (Ogata and Katsura, 1993) to fit the MFD, yielding the following parameter values: $\beta = 2.132$, $\mu = 1.784$, and $\sigma = 0.352$. Consequently, the b-value during the study period was determined to be 0.926. Furthermore, based on the approximate relationship between the minimum completeness magnitude (M_c) and parameters μ and σ, we estimated $M_c \approx \mu + 2\sigma = 2.5$. For the calculation of b-values, we employed a finite-boundary Voronoi grid partitioning technique to construct the spatial model. We considered various grid numbers (N_v) ranging from 2 to 100 and conducted 100 random realizations for each grid number. During the model selection phase, we identified the top 10% of models with the lowest BIC values as the optimal models. The median of the b-value results obtained from this selected ensemble of models was employed as the final b-value estimate. In the computation of the CMP, we divided the study area into 0.2° × 0.2° grids and set $r_0 = 120$ km as the reference distance for the Gaussian kernel function smoothing.

Results

In the computation of the b-value, the terminal time of the calculation period was fixed at 6 February 2023 00:00:00, preceding the M_w 7.8–7.6 earthquake doublet. The starting time was set for each of the 10 periods as 6 February 2013, 6 February 2014, …, 6 February 2022. As an illustrative example of the results, Figure 2a, 2c, and 2e presents the b-values for three starting times: 6 February 2013, 6 February 2018, and 6 February 2022, respectively, and Figure 2b,d,f presents the corresponding median absolute deviation (MAD). The results demonstrate that the b-values during the various periods primarily ranged from 0.6 to 1.2, exhibiting distinct spatial distribution disparities. Notably, the results for each period exhibit two key features. First, the b-values within the study area gradually decrease toward the M_w 7.8–7.6 earthquake doublet, manifesting a prominent temporal variation. For instance, the b-value near the epicenters of the M_w 7.8–7.6 earthquake doublet steadily decreases from ∼1.0 to ∼0.85 as the starting time approaches the occurrence time of the earthquake doublet. Second, a prolonged, stable low-b-value spatial heterogeneity around the future fault rupture zones, commonly employed in previous studies to identify nucleation zones of major earthquakes, is notably absent, and its application remains widely debated.

To examine the spatiotemporal evolution of b-values, we posit that the b-values within the period from 6 February 2013 to 6 February 2017, which precedes the M_w 7.8–7.6 earthquake doublet, can represent the region's background values and serve as a comparative baseline. The selection of this four-year period is influenced by a balanced consideration of sufficient data for computation and minimal overlap with the time frame of b-value temporal variations. To validate the stability of the background value results, we conducted multiple calculations by randomly extracting data within two-year windows from this period. The outcomes indicate a strong similarity in the b-values obtained from these extracted time frames. The corresponding distribution of background b-values and MAD are depicted in Figure 2g and 2h, respectively. Furthermore, by subtracting the computed b-values of the 10 periods from the background b-values, we derived the spatial distribution of Δb-values. Figure 3 presents examples of these results corresponding to the three time periods illustrated in Figure 2. The spatial distribution of Δb-values further verifies the gradual reduction in b-values across the entire study area leading up to the occurrence of the M_w 7.8–7.6 earthquake doublet. Specifically, all the periods exhibit that Δb mainly ranges [−0.3, 0], with Δb-values progressively decreasing. In addition, although the Δb-value near the epicenter of the M_w 7.8–7.6 earthquake doublet has decreased to approximately −0.20 by the starting time of 6 February 2022, it does not represent the lowest value across all periods.

Employing the Δb-values from the 10 periods, we calculated the CMP. Adhering to common practice, we set the range of Δb-values as [min(Δb), 0] and computed the resulting *Prob* distribution, illustrated in Figure 4c. The outcomes reveal elevated *Prob* distributed along the EAFZ, where the M_w 7.8–7.6 earthquake doublet is located, indicating quantifiable CMP phenomena prior to the earthquake. However, similarly high *Prob* values are also broadly distributed in the southwestern region of the study area, where no significant earthquakes occurred. Naively, spatially extensive higher Δb "anomalous" points should lead to a wider spatial distribution range for the CMP phenomenon. Therefore, to calculate the average error distance ε and coverage rate f, we set the Δb-value ranges as [−0.3, 0], [−0.2, 0], and [−0.15, 0] and recalculated the spatial distribution of *Prob*, as shown in Figure 4d, 4e,

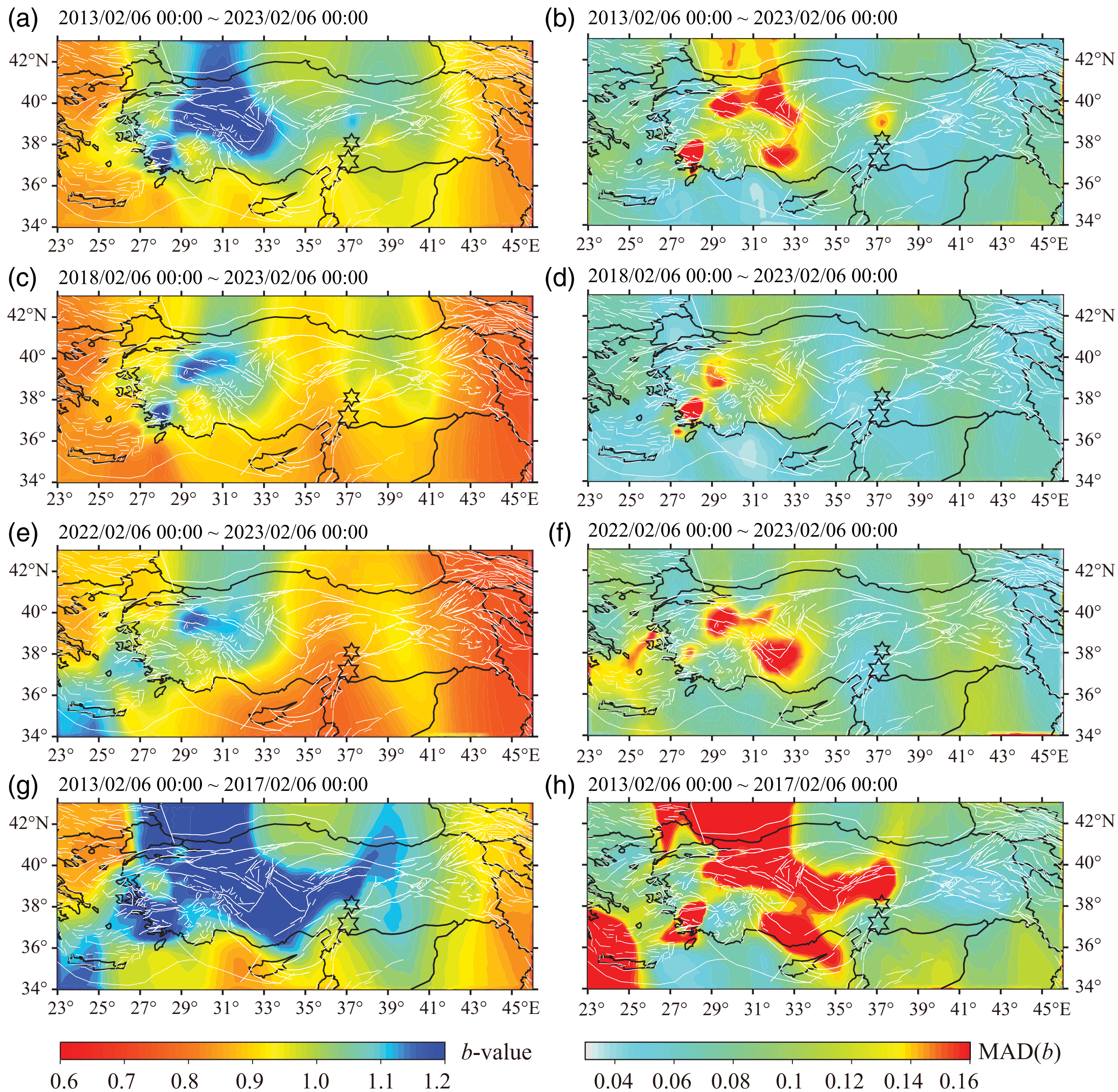

Figure 2. Distribution of *b*-values and corresponding median absolute deviation (MAD) during different time periods prior to the occurrence of the M_w 7.8–7.6 earthquake doublet. (a,c,e,g) The distribution of *b*-values during different periods, with different start times marked on each panel. (b,d,f,h) The distribution of MAD corresponding to the *b*-values during the different periods marked on each panel. Two stars indicate the epicenter of the 2023 M_w 7.8–7.6 Kahramanmaraş earthquake doublet.

and 4f, respectively. The results reveal that as the Δb-value range narrows and approaches 0, the range of elevated *Prob* values near the epicenter of the M_w 7.8–7.6 earthquake doublet expands and becomes the most distinct distribution area within the study region. Conversely, the high-value area in the southwestern region significantly contracts, accompanied by a decreasing maximum value, indicating that these regions do not align with the preparatory processes of a strong earthquake.

To validate the reliability of the computational results in this study, a series of tests were conducted, with detailed descriptions provided in the supplemental materials. For the robustness verification of the *b*-value results, we randomly sampled 75%, 50%, and 25% of models from the optimal models, as well as selected the top 75%, top 50%, and top 25% models based on their BIC values. Subsequently, we recalculated the *b*-values and assessed the robustness of the results

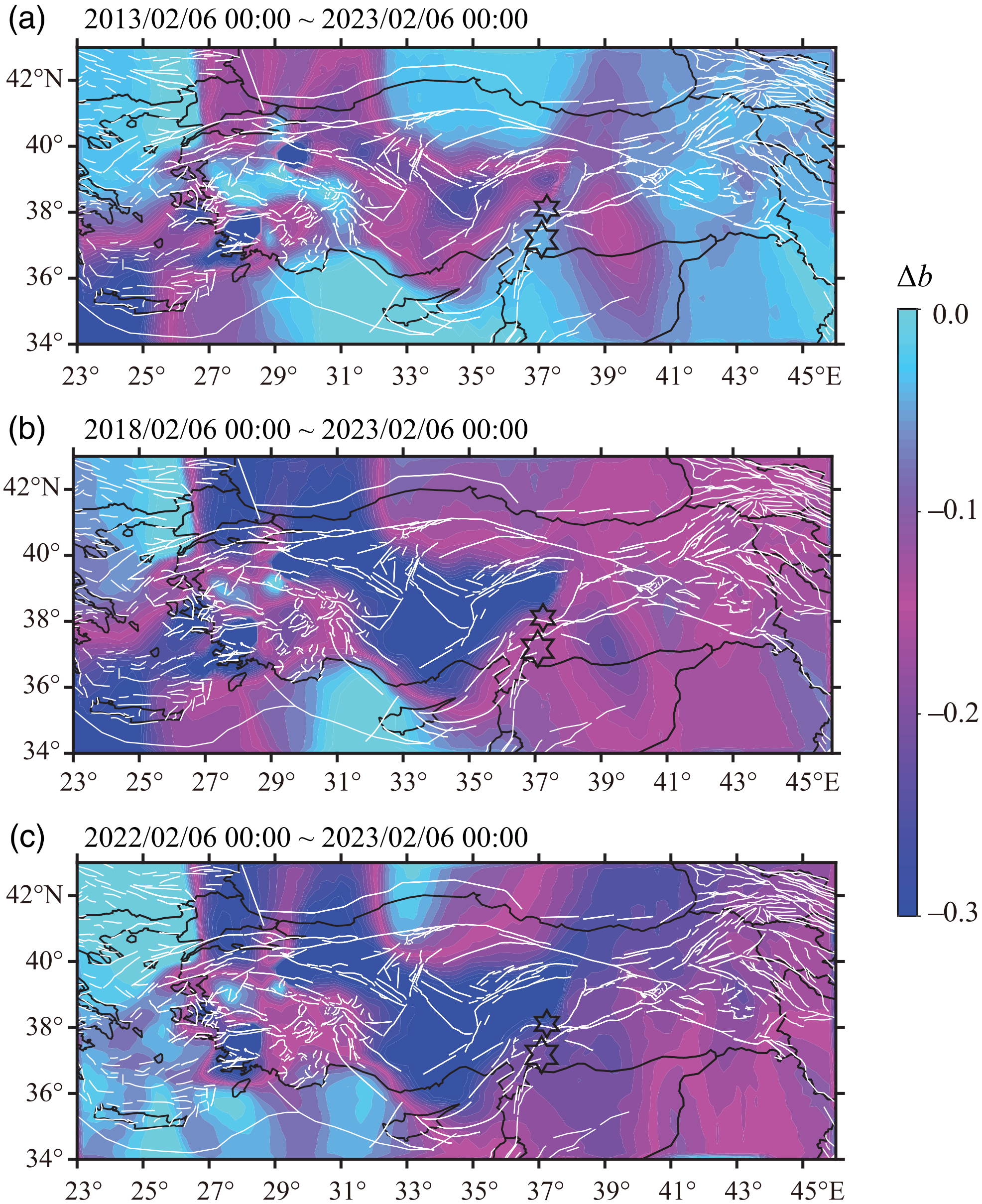

Figure 3. Distribution of the differences Δb between the b-values at various time intervals and the background b-value. (a) Differences Δb between the b-value and the background b-value for the period from 6 February 2013 to the occurrence of the earthquake doublet. (b) Differences Δb between the b-value and the background b-value for the period from 6 February 2018 to the occurrence of the earthquake doublet. (c) Differences Δb between the b-value and the background b-value for the period from 6 February 2022 to the occurrence of the earthquake doublet. The epicenters of the 2023 M_w 7.8–7.6 Kahramanmaraş earthquake doublet are indicated by the two stars.

(see Fig. S1, available in the supplemental material to this article). To examine the stability of the background b-values used for Δb calculation during the period 6 February 2013 to ∼6 February 2017, additional calculations were performed for two subperiods: 6 February 2013 to ∼6 February 2015 and 6 February 2015 to ∼6 February 2017, and a comparative analysis was conducted (see Fig. S2). Three aspects were considered to validate the reasonableness of the CMP calculation results. First, taking the results with $\Delta b \geq -0.3$ in Figure 4d as an example, a verification analysis was conducted for the b-values, Δb-values, and the integrated error distance ε_{erea} evolving over time at different spatial locations near the epicenters of earthquake doublets (see Fig. S3). Second, an analysis was performed on the impact of the 24 January 2020 M_w 6.7 Elazığ earthquake and its aftershocks, located approximately 160 km from the earthquake doublets, on the CMP calculation results (see Fig. S4). Finally, 100 random experiments were conducted to assess the potential impact of b-value errors on CMP calculation results (see Fig. S5). The results of these tests and validations collectively support the reasonableness of the computational outcomes in this study.

Discussion

As to the physical significance of the CMP phenomenon prior to the 2023 M_w 7.8–7.6 Kahramanmaraş earthquake doublet, we posit that it reflects the cumulative growth process of differential stress in the crust near the future nucleation point of a major earthquake. First, in the design of our technical approach, we employ the change in Δb-value as a metric for measuring seismic activity anomalies in CMP. This choice is grounded in laboratory studies that have established an inverse relationship between the b-value describing the MFD characteristics and the differential stress in the crust, where a reduction in the b-value is associated with increased stress (Scholz, 1968). This allows for inferring the stress state underground by directly measuring the variation in b-values. However, the magnitude of b-values may be influenced by various factors, such as crustal stress conditions (e.g., Wyss, 1973;

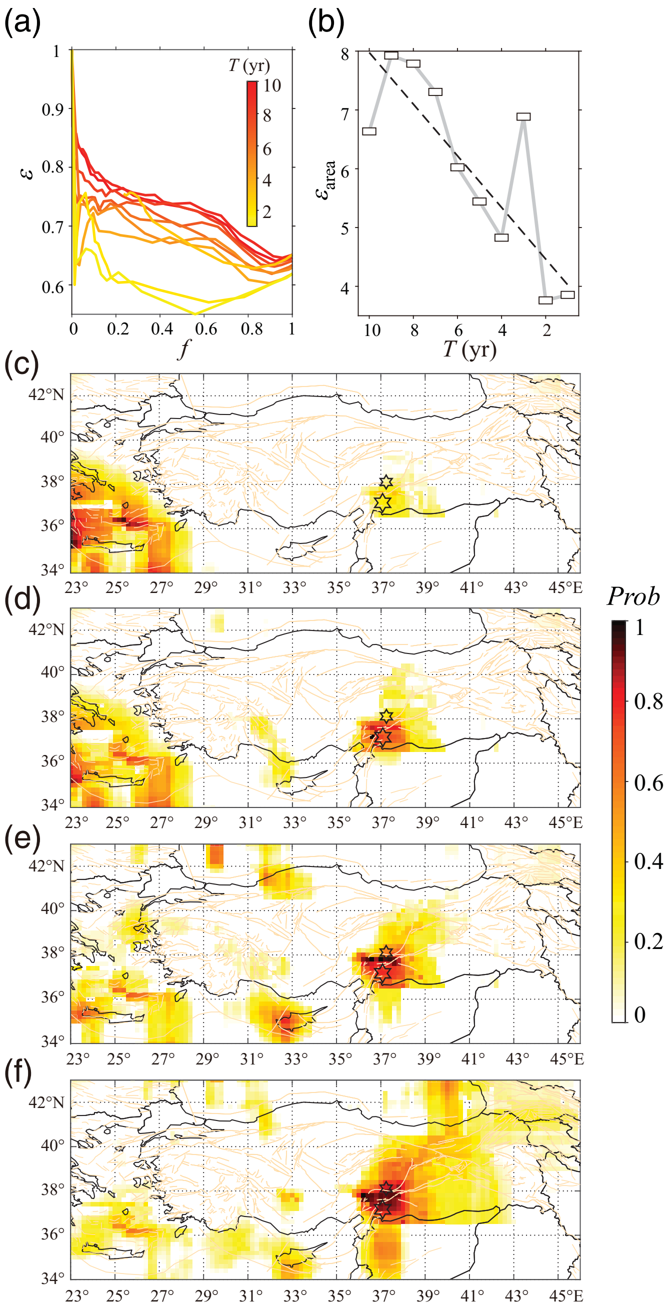

Figure 4. Cumulative migration pattern (CMP) before the 2023 M_w 7.8–7.6 Kahramanmaraş earthquake doublet. (a) Curves depicting the average error distance ε and coverage rate f for the epicenter location of the example M_w 7.8 earthquake, with different colors corresponding to various time scales T before the occurrence of the earthquake doublet. (b) Relationship between the integrated error distance ε_{erea} and time scale T for the example M_w 7.8 earthquake epicenter, with the dashed line indicating the linear fitting result and its slope representing the degree of CMP. (c–f) Distribution of normalized strong seismic hazard probability (*Prob*) obtained from CMP results using different Δb thresholds ($\Delta b \geq -0.4$, $\Delta b \geq -0.3$, $\Delta b \geq -0.2$, $\Delta b \geq -0.15$). The calculation period used was from 6 February 2013 to the occurrence of the earthquake doublet. In panels (c)–(f), colors represent the spatially normalized strong seismic hazard probability obtained from CMP results. The two stars indicate the positions of the 2023 M_w 7.8–7.6 Kahramanmaraş earthquake doublet.

Toda *et al.*, 1998), the complexity of fault traces (Stirling *et al.*, 1996), and the degree of creep (Amelung and King, 1997). Furthermore, different types of faults with distinct sliding characteristics and mechanisms exhibit characteristic distributions of b-values, with thrust faults having the lowest b-values, normal faults having the highest, and strike-slip faults being intermediate (Schorlemmer *et al.*, 2005). Therefore, employing Δb enables a more objective description of the evolution of underground stress states, ensuring conceptual clarity in the physical significance of this study's approach. In terms of observational results, over the decade preceding the 2023 M_w 7.8–7.6 Kahramanmaraş earthquake doublet, there was a widespread decrease in b-values in the study area, accompanied by the occurrence of CMP phenomena near the epicenters of the earthquake doublet. The trend changes in this region correspond to those near the nucleation point, enhancing the reliability of the physical correlation with the preparation process for a major earthquake.

The recognition in this study with regard to the quantifiable description of the preparation process for the 2023 M_w 7.8–7.6 Kahramanmaraş earthquake doublets revealed by the CMP phenomenon holds particular scientific significance, especially considering its occurrence in a complex intraplate tectonic region. Presently proposed physical models for the preparatory processes preceding major earthquakes, including cascade, preslip, and progressive or migratory localization (Ellsworth and Beroza, 1995; McLaskey, 2019; Kato and Ben-Zion, 2020), struggle to individually explain the complex spatiotemporal phenomena arising from fault interactions, volumetric processes, heterogeneous fault properties, and others. These challenges emphasize the significant scientific importance of identifying preparatory processes through observational data (Wu *et al.*, 2008; Jiang and Wu, 2011; Fielding *et al.*, 2013; Melgar *et al.*, 2020; Taymaz, Ganas, *et al.*, 2022; Taymaz, Yolsal-Çevikbilen, *et al.*, 2022). The identification of clues regarding the preparatory processes of major earthquakes on a broad spatial scale serves as an exciting entry point for validating physical models and understanding physical processes. Quantitatively characterizing the migration pattern phenomenon prior to the 2023 M_w 7.8–7.6 Kahramanmaraş earthquake doublet reveals stress transfer processes along the complex fault system of the EAFZ. This unveils valuable insights into the convergence and deformation patterns of the Eurasian, African, and Arabian plates within this region, as well as mechanisms of fault interactions.

An important technical exploration in this study involves the configuration of Δb-values within different threshold ranges and the calculation of the corresponding probability (*Prob*) for CMP. Moreover, this approach uniquely identifies the location of nucleation zones for future major earthquakes, a valuable contribution to practical seismic hazard analysis and earthquake preparedness decision-making. However, it is crucial to observe that the rupture nucleation zones provided in this study are not precise nucleation points and cannot precisely elucidate the cascade or pre-slip processes preceding rupture on adjacent faults. In addition, from a more cautious perspective, there is another significant data source in the study area, namely the Turkish Disaster and Emergency Management Authority (AFAD) earthquake catalog. Although the KOERI earthquake catalog employed in this study ensures the reliability of the conclusions, it remains essential to compare the details of earthquake preparation processes revealed by different data sources, including the AFAD earthquake catalog. Consequently, these limitations hinder a comprehensive delineation of the mechanisms driving major earthquake occurrences. Indeed, even for a single strong earthquake, its preparatory processes may involve diverse mechanical mechanisms. For instance, before the 2006 L'Aquila earthquake, aseismic processes and stress transfer processes occurred on distinct fault segments with different physical characteristics and temporal scales (Cabrera *et al.*, 2022).

In addition, this study introduces viewpoints on the academic controversy with respect to the spatiotemporal heterogeneity of b-values. Ongoing debates persist regarding the temporal decrease in b-values preceding strong earthquakes. On the one hand, numerous actual earthquake cases (Gulia and Wiemer, 2019; Xie *et al.*, 2019, 2022; Bi *et al.*, 2023), along with observations of decreasing b-values in rock fracturing experiments before instability (Thompson *et al.*, 2006; Lei, 2019), have been reported. Conversely, opposing views argue that this temporal change lacks statistical significance and should be treated as a spatially heterogeneous yet temporally stable phenomenon suitable for identifying fault asperities (Wiemer and Wyss, 2002; Schorlemmer *et al.*, 2004). Our findings demonstrate that over the decade leading to the 2023 M_w 7.8–7.6 Kahramanmaraş earthquake doublet, b-values across the entire study area exhibited a conspicuous and sustained reduction. Nevertheless, it is crucial to observe that the region near the epicenter of the earthquake doublet does not manifest the most pronounced reduction in b-values across the entire study area. This implies that the ideal model based on the traditional spatiotemporal heterogeneity assumption of b-values cannot accurately assess the precursory hazard of the 2023 M_w 7.8–7.6 Kahramanmaraş earthquake doublet, especially in determining the nucleation location. However, a new perspective provided by quantitatively describing the spatiotemporal migration of Δb reveals the most prominent migration pattern in the study area near the epicenter of the earthquake doublet. This offers a fresh research perspective for earthquake hazard assessments involving such multi-fault triggering scenarios (Jia *et al.*, 2023).

Conclusions

To investigate whether a recognizable strong earthquake preparation process existed on a large spatial scale before the occurrence of the 2023 M_w 7.8–7.6 Kahramanmaraş earthquake doublet, we utilized concepts and phenomena with clearer physical meanings. These include the spatial–temporal variation of b-values, which are inversely proportional to the difference in stress level in the crust, and the potential occurrence of CMP near the epicenter shortly before the mainshock. To ensure objectivity in b-value calculation, a data-driven method and model selection approach based on the BIC were employed. The difference between b-values and background b-values (Δb-values) was used as an "anomaly," and the degree of spatially normalized CMP (*Prob*) was calculated as an indicator of a strong seismic hazard. The findings of this study can be summarized as follows.

On a decadal timescale before the earthquake doublet, the b-values in the study area exhibited a spatially consistent decrease near the mainshock's occurrence time. The distribution of Δb within the range of $-0.4 < \Delta b < 0$ indicated a gradual enhancement of crustal difference stress on a large spatial scale. However, the Δb-values in the EAF, where the M_w 7.8–7.6 earthquake doublet occurred were not the most significant low values. Moreover, there was no prominent and long-term stable spatial heterogeneity on the EAF compared to other fault zones in the study area, making it challenging to explain using the asperity model. Further calculations have revealed the presence of CMP phenomena along the EAF, with high probability values concentrated primarily near the epicenters of the earthquake doublet. This observation not only unveils the measurable CMP phenomena preceding the occurrence of the 2023 M_w 7.8–7.6 Kahramanmaraş earthquake doublet but also indicates a physical correlation between CMP phenomena and the preparatory processes of significant earthquakes.

Given the gradual increase of crustal difference stress with quantifiable CMP phenomena on a large spatial scale, the well-defined physical significance of CMP, and its potential in forecasting the future nucleation points and relative migration degrees of strong earthquake rupture, this case study contributes to understanding the preparation processes before the occurrence of the 2023 M_w 7.8–7.6 Kahramanmaraş earthquake doublet. Furthermore, the identified CMP phenomenon holds potential as a scientific reference for mitigating similar destructive earthquakes. Nevertheless, the generality of this CMP phenomenon requires further case studies to explore its applicability and operability.

Data and Resources

The earthquake catalog for this study was obtained from the Kandilli Observatory and Earthquake Research Institute (KOERI; http://www.koeri.boun.edu.tr/sismo/2/earthquake-catalog/, last accessed May 2023). Details of data availability and usage policies can be found on the provided website. The supplemental material to this article includes a series of validations for the reliability of cumulative migration pattern (CMP) calculation results, with detailed information available in the supplemental material.

Declaration of Competing Interests

The authors acknowledge that they have no conflicts of interest recorded.

Acknowledgments

The authors would like to express their gratitude for the financial support provided by the National Key R&D Program of China (Grant Number 2023YFC3012005) and the National Natural Science Foundation of China (Grant Number U2039204). This research was conducted as part of the collaborative scientific investigation on the 2023 M_w 7.8–7.6 Kahramanmaraş earthquake doublet between the China Earthquake Administration (CEA) and the Disaster and Emergency Management Authority of Türkiye (AFAD). The authors acknowledge the valuable contributions and cooperation from both organizations during the course of this study. The authors sincerely appreciate the constructive feedback from the editors and three anonymous reviewers, which has significantly contributed to improving the quality of this article.

References

Aktug, B., H. Ozener, A. Dogru, A. Sabuncu, B. Turgut, K. Halicioglu, O. Yilmaz, and E. Havazli (2016). Slip rates and seismic potential on the east Anatolian fault system using an improved GPS velocity field, *J. Geodynam.* **94–95,** 1–12, doi: 10.1016/j.jog.2016.01.001.

Amelung, F., and G. King (1997). Earthquake scaling laws for creeping and non-creeping faults, *Geophys. Res. Lett.* **24,** no. 5, 507–510, doi: 10.1029/97GL00287.

Barbot, S., H. Luo, T. Wang, Y. Hamiel, O. Piatibratova, M. T. Javed, C. Braitenberg, and G. Gurbuz (2023). Slip distribution of the February 6, 2023 M_w 7.8 and M_w 7.6, Kahramanmaraş, Turkey earthquake sequence in the east Anatolian fault zone, *Seismica* **2,** no. 3, 1–17, doi: 10.26443/seismica.v2i3.502.

Bayrak, E., Ş. Yılmaz, M. Softa, T. Türker, and Y. Bayrak (2015). Earthquake hazard analysis for east Anatolian fault zone, Turkey, *Nat. Hazards* **76,** 1063–1077, doi: 10.1007/s11069-014-1541-5.

Bi, J. M., F. L. Yin, C. S. Jiang, X. X. Yin, Y. Ma, and C. Song (2023). Strong Aftershocks Traffic Light System (SATLS): A case study of the 8 January 2022 M_S6.9 Menyuan earthquake, Qinghai Province, China, *Front. Earth Sci.* **10,** 994850, doi: 10.3389/feart.2022.994850.

Bulut, F., M. Bohnhoff, T. Eken, C. Janssen, T. Kılıç, and G. Dresen (2012). The east Anatolian fault zone: Seismotectonic setting and spatiotemporal characteristics of seismicity based on precise earthquake locations, *J. Geophys. Res.* **117,** no. B7, doi: 10.1029/2011JB008966.

Cabrera, L., P. Poli, and W. B. Frank (2022). Tracking the spatio-temporal evolution of foreshocks preceding the M_w 6.1 2009 L'Aquila earthquake, *J. Geophys. Res.* **127,** e2021JB023888, doi: 10.1029/2021JB023888.

Cambaz, M. D., F. Turhan, M. Yılmazer, K. Kekovalı, Ö. Necmioğlu, and D. Kalafat (2019). A review on Kandilli Observatory and Earthquake Research Institute (KOERI) seismic network and earthquake catalog: 2008–2018, *Adv. Geosci.* **51,** 15–23, doi: 10.5194/adgeo-51-15-2019.

Confal, J. M., M. J. Bezada, T. Eken, M. Faccenda, E. Saygin, and T. Taymaz (2020). Influence of upper mantle anisotropy on isotropic P-wave tomography images obtained in the eastern Mediterranean region, *J. Geophys. Res.* **125,** no. 8, e2019JB018559, doi: 10.1029/2019JB018559.

Ding, H. Y., Y. J. Zhou, Z. X. Ge, T. Taymaz, A. Ghosh, H. Y. Xu, T. S. Irmak, and X. D. Song (2023). High-resolution seismicity imaging and early aftershock migration of the 2023 Kahramanmaraş (SE Türkiye) M_w 7.9 & 7.8 earthquake doublet, *Earthq. Sci.* **6,** no. 6, 417–432, doi: 10.1016/j.eqs.2023.06.002.

Ding, X., S. Xu, Y. Xie, M. van den Ende, J. Premus, and J. P. Ampuero (2023). The sharp turn: Backward rupture branching during the 2023 M_w 7.8 Kahramanmaraş (Türkiye) earthquake, *Seismica* **2,** no. 3, doi: 10.26443/seismica.v2i3.1083.

Duman, T. Y., and Ö. Emre (2013). *The East Anatolian Fault: Geometry, Segmentation and Jog Characteristics*, Geological Society, London, Special Publications, Vol. 372, 495–529, doi: 10.1144/SP372.1.

Eken, T., M. T. Qashqai, C. Schiffer, T. Taymaz, and E. Saygin (2021). New insights into crustal properties of Anatolia and its surroundings inferred from P-coda autocorrelation inversions, *J. Geophys. Res.* **126,** no. 12, e2021JB023184, doi: 10.1029/2021JB023184.

Ellsworth, W. L., and G. C. Beroza (1995). Seismic evidence for an earthquake nucleation phase, *Science* **268,** no. 5212, 851–855, doi: 10.1126/science.268.5212.851.

Fichtner, A., E. Saygin, T. Taymaz, P. Cupillard, Y. Capdevillee, and J. Trampert (2013). The deep structure of the north Anatolian fault zone, *Earth Planet. Sci. Lett.* **373,** 109–117, doi: 10.1016/j.epsl.2013.04.027.

Fielding, E. J., P. R. Lundgren, T. Taymaz, S. Yolsal-Çevikbilen, and S. E. Owen (2013). Fault-slip source models for the 2011 M7.1 Van earthquake in Turkey from SAR interferometry, pixel offset tracking, GPS and seismic waveform analysis, *Seismol. Res. Lett.* **84,** no. 4, 579–593, doi: 10.1785/0220120164.

Gabriel, A.-A., T. Ulrich, M. Marchandon, J. Biemiller, and J. Rekoske (2023). 3D dynamic rupture modeling of the 6 February 2023, Kahramanmaraş, Turkey M_w 7.8 and 7.7 earthquake doublet using early observations, *Seism. Record* **3,** no. 4, 342–356, doi: 10.1785/0320230028.

Goldberg, D. E., T. Taymaz, N. G. Reitman, A. E. Hatem, S. Yolsal-Çevikbilen, W. D. Barnhart, T. S. Irmak, D. J. Wald, T. Öcalan, W. L. Yeck, *et al.* (2023). Rapid characterization of the February 2023 Kahramanmaraş, Türkiye, earthquake sequence, *Seism. Record* **3,** no. 2, 156–167, doi: 10.1785/0320230009.

Gulia, L., and S. Wiemer (2019). Real-time discrimination of earthquake foreshocks and aftershocks, *Nature* **574,** 193–199, doi: 10.1038/s41586-019-1606-4.

Güvercin, S. E., H. Karabulut, A. Ö. Konca, U. Doğan, and S. Ergintav (2022). Active seismotectonics of the east Anatolian fault, *Geophys. J. Int.* **230,** no. 1, 50–69, doi: 10.1093/gji/ggac045.

Hall, S. (2023). What Turkey's earthquake tells us about the science of seismic forecasting, *Nature* **615,** no. 7952, 388–389, doi: 10.1038/d41586-023-00685-y.

Hussain, E., T. J. Wright, R. J. Walters, D. Bekaert, R. Lloyd, and A. Hooper (2018). Constant strain accumulation rate between major earthquakes on the north Anatolian fault, *Nat. Commun.* **9,** 1392, doi: 10.1038/s41467-018-03739-2.

Jia, Z., Z. Y. Jin, M. Marchandon, T. Ulrich, A. Gabriel, W. Y. Fan, P. Shearer, X. Y. Zou, J. Rekoske, F. Bulut, *et al.* (2023). The complex dynamics of the 2023 Kahramanmaraş, Turkey, M_w 7.8-7.7 earthquake doublet, *Science* eadi0685, doi: 10.1126/science.adi0685.

Jiang, C. S., and Z. L. Wu (2011). Intermediate-term medium-range accelerating moment release (AMR) priori to the 2010 Yushu M_S7.1 earthquake, *Chin. J. Geophys.* **54,** no. 6, 1501–1510, doi: 10.3969/j.issn.0001-5733.2011.06.009 (in Chinese).

Jiang, C. S., L. B. Han, F. Long, G. Lai, F. Yin, J. Bi, and Z. Si (2021). Spatiotemporal heterogeneity of *b* values revealed by a data-driven approach for June 17, 2019 M_S 6.0, Changning Sichuan, China earthquake sequence, *Nat. Hazards Earth Syst. Sci.* **21,** no. 7, 2233–2244, doi: 10.5194/nhess-21-2233-2021.

Kalafat, D., Y. Güneş, K. Kekovalı, M. Kara, P. Deniz, and M. Yılmazer (2011). *Bütünleştirilmiş Homojen Türkiye Deprem Kataloğu*, Boğaziçi Universitesi, Bebek, İstanbul.

Karabulut, H., S. Ezgi Güvercin, J. Hollingsworth, and A. Özgün Konca (2023). Long silence on the east Anatolian fault zone (southern Turkey) ends with devastating double earthquakes (6 February 2023) over a seismic gap: Implications for the seismic potential in the eastern Mediterranean region, *J. Geol. Soc.* **180,** no. 3, doi: 10.1144/jgs2023-021.

Kato, A., and Y. Ben-Zion (2020). The generation of large earthquakes, *Nat. Rev. Earth Environ.* **2,** 1–14, doi: 10.1038/s43017-020-00108-w.

Kawamura, M., Y.-H. Wu, T. Kudo, and C.-C. Chen (2013). Precursory migration of anomalous seismic activity revealed by the pattern informatics method: A case study of the 2011 Tohoku earthquake, Japan, *Bull. Seismol. Soc. Am.* **103,** no. 2B, 1171–1180, doi: 10.1785/0120120094.

Köküm, M., and M. İnceöz (2018). Structural analysis of the northern part of the east Anatolian fault system, *J. Struct. Geol.* **114,** 55–63, doi: 10.1016/j.jsg.2018.06.016.

Lei, X. L. (2019). Evolution of *b*-value and fractal dimension of acoustic emission events during shear rupture of an immature fault in Granite, *Appl. Sci.* **9,** no. 12, 2498, doi: 10.3390/app9122498.

Liu, C., T. Lay, R. Wang, T. Taymaz, Z. Xie, X. Xiong, T. S. Irmak, M. Kahraman, and C. Erman (2023). Complex multi-fault rupture and triggering during the 2023 earthquake doublet in southeastern Türkiye, *Nat. Commun.* **14,** 5564, doi: 10.1038/s41467-023-41404-5.

Liu, M., S. Stein, and H. Wang (2011). 2000 years of migrating earthquakes in North China: How earthquakes in midcontinents differ from those at plate boundaries, *Lithosphere* **3,** no. 2, 128–132, doi: 10.1130/L129.1.

Lyberis, N., T. Yürür, J. Chorowicz, E. Kasapoğlu, and N. Gündoğdu (1992). The east Anatolian fault: An oblique collisional belt, *Tectonophysics* **204,** 1–15.

Mai, P. M., T. Aspiotis, T. A. Aquib, E. V. Cano, D. Castro-Cruz, A. Espindola-Carmona, B. Li, X. Li, J. Liu, R. Matrau, *et al.* (2023). The destructive earthquake doublet of 6 February 2023 in south-central Türkiye and northwestern Syria: Initial observations and analyses, *Seism. Record* **3,** no. 2, 105–115, doi: 10.1785/0320230007.

McLaskey, G. C. (2019). Earthquake initiation from laboratory observations and implications for foreshocks, *J. Geophys. Res.* **124,** no. 12, 12,882–12,904, doi: 10.1029/2019JB018363.

Melgar, D., A. Ganas, T. Taymaz, S. Valkaniotis, B. Crowell, V. Kapetanidis, V. Tsironi, O. , and T. Yolsal-Çevikbilen (2020). Rupture kinematics of January 24, 2020 Mw 6.7 Doğanyol-Sivrice, Turkey earthquake on the east Anatolian fault zone imaged by space geodesy, *Geophys. J. Int.* **223,** no. 2, 862–874, doi: 10.1093/gji/ggaa345.

Melgar, D., T. Taymaz, A. Ganas, B. Crowell, T. Öcalan, M. Kahraman, V. Tsironi, S. Yolsal-Çevikbil, S. Valkaniotis, T. S. Irmak, *et al.* (2023). Sub- and super-shear ruptures during the 2023 M_w 7.8 and M_w 7.6 earthquake doublet in SE Türkiye, *Seismica* **2,** no. 3, doi: 10.26443/seismica.v2i3.387.

Nalbant, S. S., J. McCloskey, S. Steacy, and A. A. Barka (2002). Stress accumulation and increased seismic risk in eastern Turkey, *Earth Planet. Sci. Lett.* **195,** nos. 3/4, 291–298, doi: 10.1016/S0012-821X(01)00592-1.

Ogata, Y., and K. Katsura (1993). Analysis of temporal and spatial heterogeneity of magnitude frequency distribution inferred from earthquake catalogues, *Geophys. J. Int.* **113,** no. 3, 727–738, doi: 10.1111/j.1365-246X.1993.tb04663.x.

Okuwaki, R., Y. Yagi, T. Taymaz, and S. P. Hicks (2023). Multi-scale rupture growth with alternating directions in a complex fault network during the 2023 south-eastern Türkiye and Syria earthquake doublet, *Geophys. Res. Lett.* **50,** no. 12, e2023GL103480, doi: 10.1029/2023GL103480.

Panet, I., S. Bonvalot, C. Narteau, D. Remy, and J. Lemoine (2018). Migrating pattern of deformation prior to the Tohoku-Oki earthquake revealed by GRACE data, *Nat. Geosci.* **11,** 367–373, doi: 10.1038/s41561-018-0099-3.

Picozzi, M., and A. Iaccarino (2023). The Preparatory process of the 2023 Mw 7.8 Turkey earthquake, 27 February 2023, PREPRINT (Version 1) available at *Research Square*, doi: 10.21203/rs.3.rs-2619572/v1.

Pousse-Beltran, L., E. Nissen, E. A. Bergman, M. D. Cambaz, É. Gaudreau, E. Karasözen, and F. Tan (2020). The 2020 M_w 6.8 Elazığ (Turkey) earthquake reveals rupture behavior of the east Anatolian fault, *Geophys. Res. Lett.* **47,** e2020GL088136, doi: 10.1029/2020GL088136.

Rebetsky, Y. L. (2023). Tectonophysical zoning of seismogenic faults in eastern Anatolia and February 6, 2023 Kahramanmaraş earthquakes, *Izv. Phys. Solid Earth* **59,** no. 6, 851–877, doi: 10.1134/s1069351323060174.

Reitman, N. G., R. W. Briggs, W. D. Barnhart, A. E. Hatem, J. A. Thompson Jobe, C. B. DuRoss, R. D. Gold, J. D. Mejstrik, C. Collett, R. D. Koehler, *et al.* (2023). Rapid surface rupture mapping from satellite data: The 2023 Kahramanmaraş, Turkey (Türkiye), earthquake sequence, *Seism. Record* **3,** no. 4, 289–298, doi: 10.1785/0320230029.

Şaroğlu, F., Ö. Emre, and İ. Kuşçu (1992). The east Anatolian fault zone of Turkey, *Ann. Tecton.* **6,** 99–125.

Scholz, C. H. (1968). The frequency-magnitude relation of microfracturing in rock and its relation to earthquakes, *Bull. Seismol. Soc. Am.* **58,** no. 1, 399–415.

Schorlemmer, D., S. Wiemer, and M. Wyss (2004). Earthquake statistics at Parkfield: 1. Stationarity of *b* values, *J. Geophys. Res.* **109,** no. B12, doi: 10.1029/2004JB003234.

Schorlemmer, D., S. Wiemer, and M. Wyss (2005). Variations in earthquake-size distribution across different stress regimes, *Nature* **437,** 539–542, doi: 10.1038/nature04094.

Si, Z. Y., and C. S. Jiang (2019). Research on parameter calculation for the Ogata–Katsura 1993 model in terms of the frequency-magnitude distribution based on a data-driven approach, *Seismol. Res. Lett.* **90,** no. 3, 1318–1329, doi: 10.1785/0220180372.

Simonov, D. A., and V. S. Zakharov (2023). Preliminary seismotectonic analysis of the catastrophic earthquake in south-eastern Turkey on February 6, 2023, *Izv. Phys. Solid Earth* **59,** no. 6, 839–850, doi: 10.1134/s1069351323060198.

Smith, W. D. (1981). The *b*-value as an earthquake precursor, *Nature* **289,** 136–139, doi: 10.1038/289136a0.

Stein, R. S., S. Toda, A. D. Özbakir, V. Sevilgen, H. Gonzalez-Huizar, G. Lotto, and S. Sevilgen (2023). Interactions, stress changes, mysteries, and partial forecasts of the 2023 Kahramanmaraş, Türkiye, earthquakes, *Temblor*, doi: 10.32858/temblor.299.

Stirling, M. W., S. G. Wesnousky, and K. Shimazaki (1996). Fault trace complexity, cumulative slip, and the shape of the magnitude-frequency distribution for strike-slip faults, a global survey, *Geophys. J. Int.* **124,** no. 3, 833–868, doi: 10.1111/j.1365-246X.1996.tb05641.x.

Styron, R., and M. Pagani (2020). The GEM global active faults database, doi: 10.1177/8755293020944182.

Taymaz, T., H. Eyidoğan, and J. Jackson (1991). Source parameters of large earthquakes in the east Anatolian fault zone (Turkey), *Geophys. J. Int.* **106,** no. 3, 537–550, doi: 10.1111/j.1365-246X.1991.tb06328.x.

Taymaz, T., A. Ganas, M. Berberian, T. Eken, T. S. Irmak, V. Kapetanidis, S. Yolsal-Çevikbilen, C. Erman, D. Keleş, C. Esmaeili, *et al.* (2022). The 23 February 2020 Qotur-Ravian earthquake doublet at the Iranian-Turkish border: Seismological and InSAR evidence for escape tectonics, *Tectonophysics* **838,** 229482, doi: 10.1016/j.tecto.2022.229482.

Taymaz, T., A. Ganas, S. Yolsal-Çevikbilen, F. Vera, T. Eken, C. Erman, D. Keleş, V. Kapetanidis, S. Valkaniotis, I. Karasante, *et al.* (2021). Source mechanism and rupture process of the 24 January 2020 M_w 6.7 Doğanyol-Sivrice earthquake obtained from seismological waveform analysis and space geodetic observations on the east Anatolian fault zone (Turkey), *Tectonophysics* **804,** 228745, doi: 10.1016/j.tecto.2021.228745.

Taymaz, T., S. Yolsal-Çevikbilen, T. S. Irmak, F. Vera, C. Liu, T. Eken, Z. Zhang, C. Erman, and D. Keleş (2022). Kinematics of the 30 October 2020 M_w 7.0 Néon Karlovásion (Samos) earthquake in the eastern Aegean Sea: Implications on source characteristics and dynamic rupture simulations, *Tectonophysics* **826,** 229223, doi: 10.1016/j.tecto.2022.229223.

Thompson, B. D., R. P. Young, and D. A. Lockner (2006). Fracture in Westerly granite under AE feedback and constant strain rate loading: Nucleation, quasi-static propagation, and the transition to unstable fracture propagation, *Pure Appl. Geophys.* **163,** nos. 5/6, 995–1019, doi: 10.1007/s00024-006-0054-x.

Toda, S., R. S. Stein, P. A. Reasenberg, J. H. Dieterich, and A. Yoshida (1998). Stress transferred by the 1995 M_w=6.9 Kobe, Japan, shock, effect on aftershocks and future earthquake probabilities, *J. Geophys. Res.* **103,** no. B10, 24,543–24,565, doi: 10.1029/98JB00765.

Toker, M., E. Yavuz, M. Utkucu, and F. Uzunca (2023). Multiple segmentation and seismogenic evolution of the 6th February 2023 (M_w 7.8 and 7.7) consecutive earthquake ruptures and aftershock deformation in the Maras triple junction region of SE-Anatolia, Turkey, *Phys. Earth Planet. In.* **345,** 107114, doi: 10.1016/j.pepi.2023.107114.

Vanacore, E. A., T. Taymaz, and E. Saygin (2013). Moho structure of the Anatolian plate from receiver function analysis, *Geophys. J. Int.* **193,** no. 1, 329–337, doi: 10.1093/gji/ggs107.

Wang, H., Z. Huang, E. Eken, D. Keleş, T. Kaya-Eken, J. M. Confal, C. Erman, S. Yolsal-Çevikbilen, D. Zhao, and T. Taymaz (2020). Isotropic and anisotropic P-wave velocity structures of the crust and uppermost mantle beneath Turkey, *J. Geophys. Res.* **125,** no. 12, e2020JB019566, doi: 10.1029/2020JB019566.

Wang, Z., W. Zhang, T. Taymaz, Z. He, T. Xu, and Z. Zhang (2023). Dynamic rupture process of the 2023 M_w 7.8 Kahramanmaraş earthquake (SE Türkiye): Variable rupture speed and implications for seismic hazard, *Geophys. Res. Lett.* **50,** e2023GL104787, doi: 10.1029/2023GL104787.

Wiemer, S., and M. Wyss (2002). Mapping spatial variability of the frequency-magnitude distribution of earthquakes, in *Advances in Geophysics*, R. Dmowska and B. Saltzman (Editors), Vol. 45, Academic Press, San Diego, California, 259–302, doi: 10.1016/S0065-2687(02)80007-3

Wu, F., J. J. Xie, Z. An, C. H. Lyu, T. Taymaz, T. S. Irmak, X. J. Li, Z. P. Wen, and B. F. Zhou (2023). Pulse-like ground motion observed during the 6 February 2023 M_w 7.8 Pazarcık earthquake (Kahramanmaraş, SE Türkiye), *Earthq. Sci.* **36,** no. 4, 328–339, doi: 10.1016/j.eqs.2023.05.005.

Wu, Y.-H., C.-C. Chen, and J. B. Rundle (2008). Detecting precursory earthquake migration patterns using the pattern informatics method, *Geophys. Res. Lett.* **35,** L19304, doi: 10.1029/2008GL035215.

Wyss, M. (1973). Towards a physical understanding of the earthquake frequency distribution, *Geophys. J. R. Astron. Soc.* **31,** no. 4, 341–359, doi: 10.1111/j.1365-246X.1973.tb06506.x.

Xie, W. Y., K. Hattori, and P. Han (2019). Temporal variation and statistical assessment of the *b* value off the Pacific Coast of Tokachi, Hokkaido, Japan, *Entropy* **21,** no. 3, 249, doi: 10.3390/e21030249.

Xie, W., K. Hattori, P. Han, and H. Shi (2022). Temporal variation of *b* value with statistical test in Wenchuan area, China prior to the 2008 Wenchuan earthquake, *Entropy* **24,** no. 4, 494, doi: 10.3390/e24040494.

Xu, C., Y. Zhang, S. Hua, X. Zhang, L. Xu, Y. Chen, and T. Taymaz (2023). Rapid source inversions of the 2023 SE Türkiye earthquakes with teleseismic and strong-motion data, *Earthq. Sci.* **36,** no. 4, 316–327, doi: 10.1016/j.eqs.2023.05.004.

Zaccagnino, D., L. Telesca, O. Tan, and C. Doglioni (2023). Clustering analysis of seismicity in the Anatolian region with implications for seismic hazard, *Entropy* **25,** no. 6, 835, doi: 10.3390/e25060835.

Zhang, Y., X. Tang, D. Liu, T. Taymaz, T. Eken, R. Guo, Y. Zheng, J. Wang, and H. Sun (2023). Geometric controls on cascading rupture of the 2023 Kahramanmaraş earthquake doublet, *Nat. Geosci.* **16,** 1054–1060, doi: 10.1038/s41561-023-01283-3.

Manuscript received 7 December 2023
Published online 19 January 2024